AN EFFICIENT METHOD TO DESIGN PREMATURE END-OF-LIFE TRAJECTORIES: A HYPOTHETICAL ALTERNATE FATE FOR CASSINI

Mar Vaquero[†] **and Juan Senent**

Jet Propulsion Laboratory, California Institute of Technology. 4800 Oak Grove Drive, Pasadena, CA 91109[*]

[†]*Corresponding Author. Tel: (818) 354-5670; Mar.Vaquero@jpl.nasa.gov*

Abstract:

What would happen if, hypothetically, the highly successful Cassini mission were to end prematurely due to shortage of propellant or sudden subsystem failure? A solid plan to quickly produce a solution for any given scenario, regardless of where the spacecraft is along its reference path, must be in place to safely dispose of the spacecraft and meet all planetary protection requirements. As a contingency plan for this hypothetical situation, a method to design viable, high-fidelity, terminating trajectories based on a hybrid approach that exploits two-body and three-body flyby transfers combined with a numerical optimization scheme is detailed in this paper.

1. Introduction

Although the majority of the times a mission is terminated in a planned fashion, sometimes the degradation of subsystems (solar arrays or thrusters) and onboard components or the lack of fuel in the tanks can force a premature disposal of the spacecraft. Planetary protection and organic contamination control requirements dictate how spacecraft disposal must be carried out at the end of the mission. These requirements, which are usually specific to the mission, are one of the driving factors in the design of controlled end-of-life trajectories. Consider the highly successful Cassini mission, which continues to explore and collect valuable scientific data with unprecedented details of the Saturnian system for over a decade now. It is known that the spacecraft will be running low on propellant in mid-to-late 2017. Several studies were carried out to design the most optimal – in terms of science return and fuel consumption – end-of-mission (EOM) scenario. Currently, the Cassini mission is proposed to end nominally with a series of 22 highly inclined (62^o), short period (6.5 days), ballistic orbits each passing within a few thousand kilometers of the cloud tops of Saturn, ultimately impacting the planet on September 15, 2017 [1]. The nominal EOM trajectory, encompassing the F-ring orbits (green), the Grand Finale orbits (blue), and the final orbit (red) culminating with Saturn atmospheric entry, is depicted in Figure 1. This end trajectory was incorporated in the final phase of the Solstice Mission after multiple tradeoff studies were carried out to ensure that, per planetary quarantine requirements and before the spacecraft runs out of propellant, the possibility of future impact with the icy moons was precluded. This particular design was selected by the different science disciplines because of its attractive geometry, which offers scientists an opportunity – otherwise unavailable – to study the intricacies of the planet's thermosphere as well as its complex ring system. However, this was certainly not the only available spacecraft disposal option. Several other end-of-life options were considered; the spacecraft could i) impact Saturn on a different path (short or long impact orbits with various inclinations) [2], ii)

remain in the Saturnian system (long-term stable orbits) [3], or iii) entirely escape the Saturnian system (large heliocentric orbits). In any case, the design of such orbits is constrained by the requirement to prevent contamination of a pristine environment and the desire to avoid collisions with any moons, particularly Titan and Enceladus. Additionally, these orbits must be accessible from the Cassini reference trajectory with minimal ΔV usage and maintain their characteristics over long-term propagation under gravitational perturbations of the Sun, Jupiter, Titan, and other moons of Saturn.

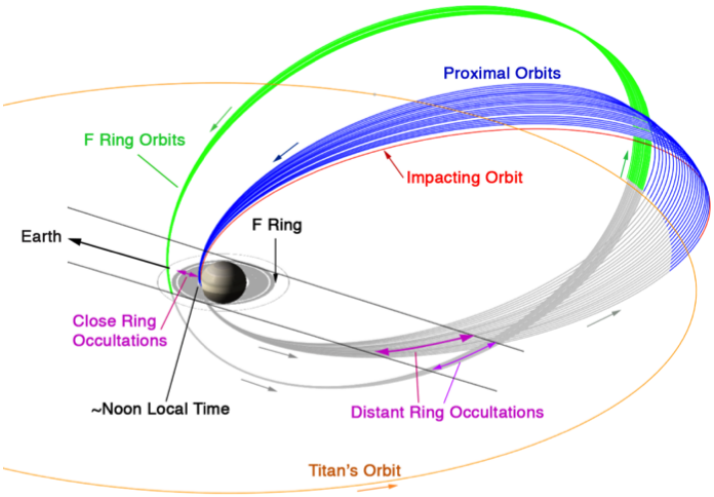

Figure 1. Representation of Cassini's end of mission encompassing the F-ring orbits (green), the Grand Finale orbits (blue), and the final orbit (red) culminating with Saturn atmospheric entry on September 15, 2017 [1].

What would happen if, hypothetically, the mission were to be ended prematurely? The current nominal EOM plan is tied to a particular future flyby geometry, initial state and time epoch and, thus, cannot be attached to the reference path at an earlier state and epoch. As the end-of-mission date approaches, both the uncertainty in usable propellant margins and the probability of spacecraft systems failure increase. If the spacecraft were to run low on propellant, or one of the propulsion subsystems were to suddenly fail, such that the engines became inoperable and control of the spacecraft was lost, a solid plan ought to be in place to safely dispose of the vehicle and meet the planetary protection requirements. This hypothetical 'emergency' situation is different from the nominal design scenario in the sense that i) no input from the science teams is taken into consideration (the priority is to safely dispose of the vehicle, not to collect science), ii) there are severe restrictions on the ΔV usage (not necessarily because of the availability of propellant, but because of the limited ability of maneuvering the spacecraft), and iii) a point solution must be quickly produced for any possible scenario, regardless of the selected initial state or the epoch along the reference trajectory. Thus, a robust method to efficiently design alternate EOM trajectories must be readily available.

A design method to produce viable terminating trajectories is detailed in this paper. The methodology is primarily based on a hybrid approach that exploits two-body and three-body resonant and non-resonant flyby transfers combined with a numerical optimization scheme within a high-fidelity simulation environment. Emphasis is given to the design process along with the differential

corrections algorithms and several end-of-mission scenarios are illustrated to demonstrate the capability of quickly computing a feasible – and hypothetical – end-of-life trajectory from a selected point along the current reference trajectory.

2. General Methodology: Dynamical Models and Assumptions

A hybrid approach is adopted to solve the problem of designing suitable, yet hypothetical, alternate impact trajectories for Cassini. This approach relies on an initial assessment of the design space in a lower-fidelity gravitational model and a subsequent refined search in a full ephemeris dynamical model. Each phase of the trajectory design process is detailed and the assumptions, constraints, and dynamical model definitions are explained in this section.

2.1. Hypothetical Problem Definition: Assumptions and Constraints

In a hypothetical scenario, the spacecraft is flying the current reference trajectory when an unexpected event (degradation of power subsystems and onboard components or the lack of fuel in the tanks) forces a premature end-of-mission. To meet planetary protection requirements, a disposal trajectory that branches off the reference trajectory must be quickly designed and the mission ended within six months of the initial detection of the problem. The following particular hypothetical scenario is specified for illustration purposes:

- A subsystem failure is detected and the starting point for the alternate end-of-life trajectory is assumed to be a few days before the Titan-115 flyby (3,817.4 km altitude) on January 16, 2016. During this time period, the reference path is almost equatorial with an average orbital inclination (with respect to the ring plane) of 1.3 degrees.
- One maneuver is designed to modify the nominal aimpoint coordinates of the Titan-115 flyby and alter the spacecraft path from the current reference trajectory to an alternate impact trajectory.
- Per planetary protection requirements, impact with selected icy moons should be avoided. In this study, impact trajectories with Saturn and Mimas are considered as viable options.
- After the maneuver is performed, the new impact trajectory is ballistic and no further maneuvers are required to guarantee safe disposal of the spacecraft.
- A minimum flyby altitude of 1,300 km is imposed to avoid transitions to RCS control during any subsequent flybys.
- The time-of-flight of the new impact trajectory must not exceed six months. This constraint is based on the fact that the spacecraft may be inoperable shortly after a subsystem failure is detected.
- Any ring crossings must be avoided as well as crossings with the moons orbital planes at the satellites's radial distance from Saturn.
- Due to limitations in the ΔV budget, the maneuver must be optimized.

The leg along the current reference trajectory being considered in this hypothetical scenario is represented in Figure 2. The time frame considered spans eight days before the T-115 flyby up to the T-116 flyby. Note that the reference path features an Enceladus flyby (E-22) prior to the Titan-115 flyby, and the spacecraft is in a 1:1 orbital resonance with Titan from Titan-115 to T-116 [4], as

illustrated in Figure 2(d). The plan is to perform a maneuver a few days before the T-115 encounter to modify the nominal aimpoint parameters and place the spacecraft on an impact trajectory (with Saturn or a non-icy moon) within six months.

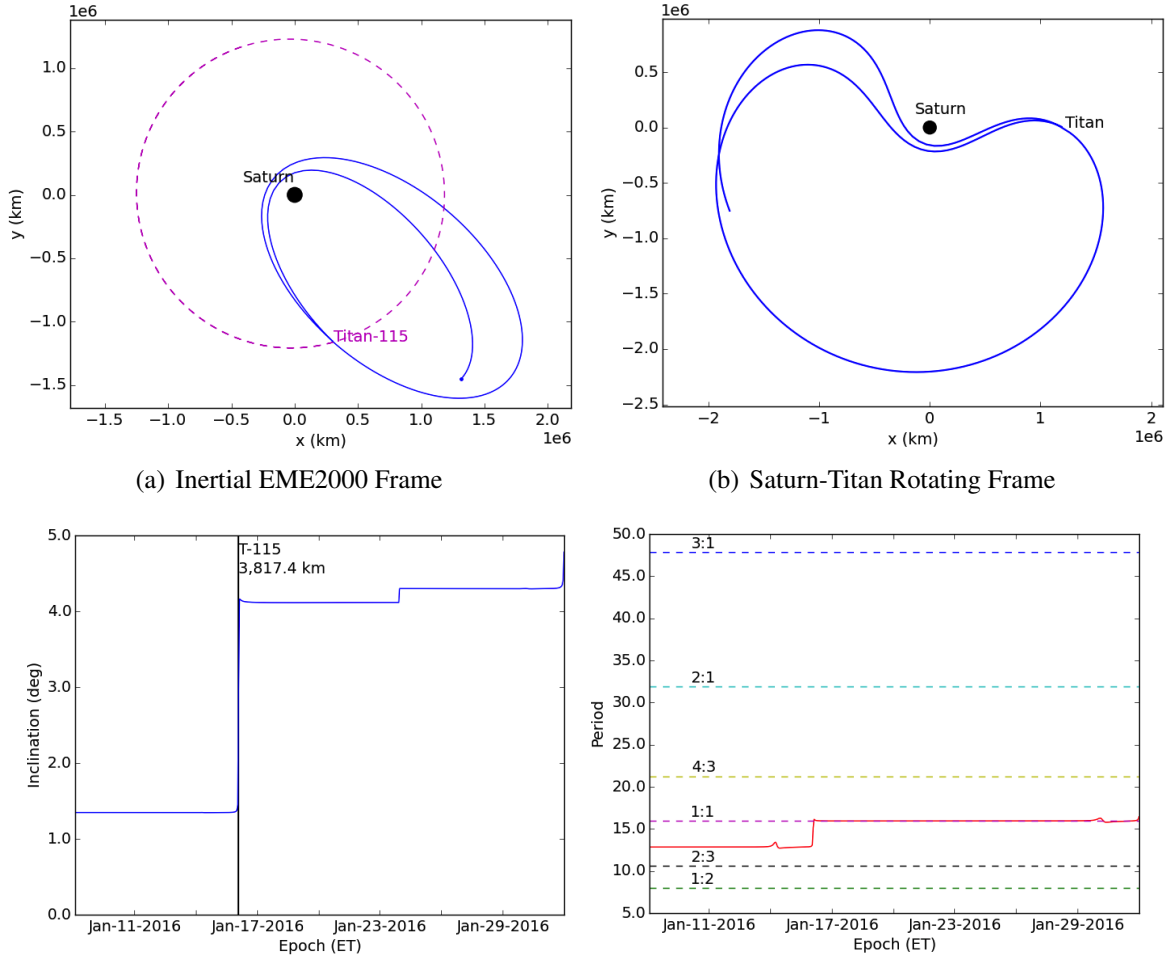

(a) Inertial EME2000 Frame

(b) Saturn-Titan Rotating Frame

(c) Orbital Inclination vs. Time

(d) Orbital Period vs. Time

Figure 2. Cassini reference trajectory from January 8, 2016 (8 days prior to T-115) to February 1, 2016 (Titan-116). The orbital path is plotted in an inertial EME2000 coordinate frame in (a) and in a Saturn-Titan rotating frame in (b). The osculating orbital inclination (with respect to the ring plane) and orbital period values as a function of time are represented in (c) and (d), respectively. The dotted lines in (d) illustrate different resonant periods with Titan.

2.2. Analysis in Different Fidelity Models

Two dynamical models are considered in this study: the Saturn-Titan Circular Restricted Three-Body (CR3BP) model and the full ephemeris model. The lower-fidelity model serves as a platform to gain insight into the design space via the application of mapping techniques and a differential corrections algorithm. Integration in the full ephemeris model is needed to refine the search and produce realistic impact trajectories that could, eventually, be flown by the spacecraft. A nonlinear optimizer is also tied to the full gravitational force model propagation and corrections scheme

to produce ΔV-optimal trajectories. A basic definition of each dynamical model and differential corrections algorithms is provided in this section.

2.2.1. The Circular Restricted Three-Body Model

The Circular Restricted Three-Body Problem serves as the basis for the initial problem formulation. In the restricted problem, the motion of an infinitesimal third particle, P_3 (spacecraft), is modeled in the presence of two gravitationally-attracting bodies of significantly larger mass, P_1 (Saturn) and P_2 (Titan). The motion of P_3 is governed by the well-known scalar, second-order differential equations of motion in standard form [5]. The state vector is defined as the six-element state vector $[x\ y\ z\ \dot{x}\ \dot{y}\ \dot{z}]^T$, where the dot indicates a derivative with respect to the nondimensional time, τ, and relative to an observer in a rotating reference frame. The mass fraction μ is associated with the two system primaries, $\mu = \frac{m_2}{m_1+m_2}$, where m_1 and m_2 are the masses of P_1 and P_2, respectively. For reference, in this analysis, the value of the mass ratio in the Saturn-Titan system is assumed to be $\mu = 2.3664 \times 10^{-4}$.

The computation of continuous multi-body impact trajectories with different itineraries and constraints in the nonlinear system involves the use of a multi-dimensional version of a Newton-Raphson differential corrections process implemented as a shooting method; in a multiple shooting algorithm, the trajectory is discretized into a series of "patch points" and multiple integrated segments are employed to satisfy the trajectory constraints. The general scheme appears in Figure 3 with the representation of an initial guess in Figure 3(a) and a converged solution in Figure 3(b). The initial path, represented via a series of intermediate arcs, is discontinuous in position and velocity. The goal is to employ the corrections algorithm to enforce continuity in all seven states, that is, position, velocity, and time. Many different formulations exist to implement a multiple shooting process. In this investigation, a straightforward free variables and constraints implementation is selected [6, 7, 8]. This approach employs a single vector update within each iteration and a single scalar criteria for convergence. It is not the only, nor the best, implementation for all applications. But, the method is quite robust and performs well for all of the examples in this study. Consider a free variable vector $\bar{X}$ comprised of a n number of state vectors and $n-1$ integration times, i.e., $\bar{X} = [\bar{x}_1\ \ ...\ \ \bar{x}_n\ \ \tau_1\ \ ...\ \tau_{n-1}]^T$. To ensure that the trajectory possesses some desired characteristics, the free variable vector is subject to m scalar constraint equations satisfying $\bar{F}(\bar{X}) = [\bar{x}_2^\tau - \bar{x}_2\ \ ..\ \ \bar{x}_n^\tau - \bar{x}_n]^T = \bar{0}$, where the vectors $\bar{x}_n^\tau$ are the final integrated states along each trajectory arc after any propagation step. To construct a smooth, continuous path, the discontinuities represented in $\bar{F}(\bar{X})$ must be removed. In the design of impact trajectories, likely quantities to be constrained include position and velocity as well as end-point constraints, such as distances or angles.

Given this problem formulation, the goal is the numerical computation of a solution $\bar{X}^*$ that satisfies the constraint equations, that is, $\bar{F}(\bar{X}^*) = \bar{0}$, within a specified tolerance. Through this iterative process, the design vector $\bar{X}$ is updated using the Jacobian matrix, that is, $D\bar{F}(\bar{X})$, which requires partial derivatives relating the variations in the constraints to the changes in the free variables. Along each arc, the partials of the end states with respect to the initial states are, in fact, simply the elements of the state transition matrix (STM). The time derivatives are evaluated at the final state along each integrated arc. If the number of free variables equals the number of constraints, a

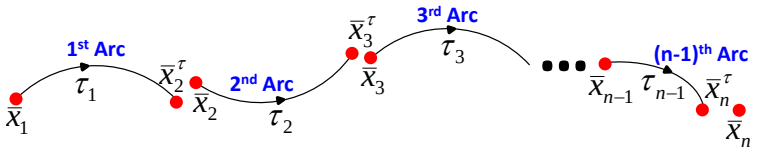

(a) Initial Guess

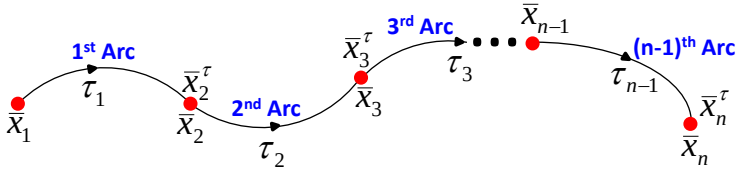

(b) Continuous Trajectory

Figure 3. Schematic of a General Multiple Shooting Algorithm [8]

unique solution is obtained via a simple multi-variable Newton's Method. If more free variables exist than constraints, infinitely many solutions exist. The selection of a single solution among all possible solutions requires the specification of some selection criteria. In this study, a solution is obtained by employing an iterative first-order minimum-norm update equation; a minimum-norm solution is selected because the difference between one iteration and the next is minimized to ensure that the converged solution remains close to the initial guess and, therefore, retains most of the characteristics of the initial guess.

2.2.2. The Restricted *n*-Body Problem

The *n*-body model, frequently formulated as an ephemeris model, is fundamental in the analysis of trajectories that support missions since it is higher-fidelity and allows for the incorporation of perturbations and additional gravitational forces that exist in the true dynamical environment. Suitable approximations for the relative locations of the celestial bodies are obtained directly from a NASA Jet Propulsion Laboratory (JPL) planetary ephemeris data file. In this study, the mutual gravity between the n point masses is assumed to be the only force acting within the system. Then, from Newton's Second Law, the equation of motion that describes the relative motion of m_1 and m_2 within a system of n bodies is derived assuming that the masses in the system are constant and all derivatives are evaluated relative to an (unaccelerated) inertial observer [9], i.e.,

$$\frac{d^2\bar{r}}{dt^2} + G\frac{(m_1+m_2)}{r^3}\bar{r} = -G\sum_{j=3}^{n} m_j \left(\frac{\bar{d}_j}{d_j^3} - \frac{\bar{\rho}_j}{\rho_j^3}\right)$$

where $\bar{r} = \bar{r}_2 - \bar{r}_1$, $\bar{\rho}_j = \bar{r}_j - \bar{r}_1$, and $\bar{d}_j = \bar{r} - \bar{\rho}_j$. In the two-body problem, all the perturbing terms on the right-hand side of the equation are removed and a closed-form analytical solution is available. However, this analytical result no longer exists if even one more body is added to the system. But, the dynamical system of equations can be numerically simulated.

3. Application to the Design of Cassini End-of-Life Trajectories

An initial assessment of the design space is done in the Saturn-Titan CR3B model via various map generation techniques combined with the application of a robust differential corrections algorithm to

produce impact trajectories that meet a subset of requirements. This process involves the propagation of a very large number of trajectories that end impacting Saturn after one, two, or three flybys with Titan. However, because of the simplicity of the model, the propagations can be done quickly and efficiently and without having any *a priori* knowledge of the solution space. These numerically integrated trajectories in the nonlinear system are then visualized on a two-dimensional map to aid in making general observations about the design trade space. Because these trajectories do not meet the full set of requirements, such as ring plane crossing constraints, a more refined search is later performed in the higher-fidelity dynamical model to produce feasible, flyable trajectories.

3.1. Maps: Initial Assessment of the Design Space

Various types of maps are useful to aid in the interpretation of the phase space in this problem. In general, maps reduce the dimensionality of the problem and are a valuable tool in the study of many different types of orbits and the natural flow in their vicinity [10, 11, 12, 13]. The concept for the construction of a general map is illustrated in Figure 4. To construct a map, a surface Σ that is transverse to the flow (and may be higher-dimensional and not necessarily defined in physical space), is defined at a particular point along the flow. In Figure 4, a periodic orbit, defined in terms of the state $\mathbf{x}$, is initiated in the plane Σ and returns to intersect exactly the same point on the plane after one period. Such a point is denoted a 'fixed point'. Then, for any point $\mathbf{x} \in \Sigma$ sufficiently close to the fixed point, a propagation of the nonlinear differential equations through $\mathbf{x}$, intersects the plane Σ again at the first return point $\mathbf{x_{i+1}}$, generally near the original fixed point. Similarly, a propagation in negative time intersects the plane Σ at $\mathbf{x_{i-1}}$.

Maps are most insightful when the appropriate set of initial conditions is selected. For instance, if the flow in the vicinity of a periodic orbit is to be explored, then a series of small perturbations in position and velocity are added to the state associated with the periodic orbit and the resulting initial conditions are propagated forward and the returns to the map recorded and visualized on the 2D surface of section to gain insight into the quasi-periodic flow in the vicinity of the periodic orbit. In this study, it is of interest to analyze trajectories with a very particular itinerary, that is, trajectories that end on impact with Saturn after at least one Titan flyby. At the very least, a Titan flyby is needed to achieve the end goal of impacting Saturn for a reasonable propellant cost. Therefore, a randomly selected set of initial conditions will not provide meaningful insight into the problem since only trajectories that impact the planet within six months are to be considered. There are different ways to construct a meaningful set of initial conditions for this particular problem, but pseudo-state theory [14] is exploited in this study.

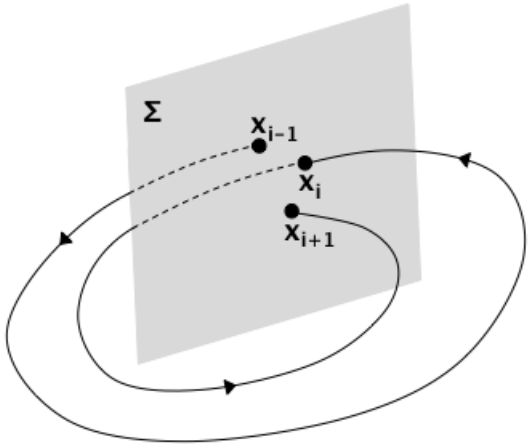

Figure 4. General Map Diagram

3.1.1. Quick Generation of Impact Flyby Trajectories via Pseudo-State Theory

Given that at least one Titan flyby is to be performed before Saturn impact, a set of initial conditions for the map can be generated based either on the conditions at Saturn impact itself or the conditions at the last Titan flyby (which inevitably ends in Saturn impact). The problem with defining initial conditions for the map at Saturn impact (and propagating these states in negative time) is that there is no control over any of Titan flybys associated with these impact trajectories. The only efficient way to reduce the ΔV is to exploit Titan's gravitational effect on the spacecraft. If there's no control on the flyby altitude, then many trajectories that require very large amounts of propellant to impact the planet end up being uselessly integrated. The alternative is to produce a set of flyby initial conditions at Titan that are guaranteed to end on Saturn impact when propagated forward in time. This is done by imposing bounds on orbital parameters such as minimum altitude, outgoing V_∞ vector magnitude, and orbital inclination before and after the flyby. These constraints are necessary to avoid ring and icy moons plane crossings as well as to maintain the orbital inclination of the incoming trajectory near the orbital plane of the reference trajectory and, thus, reduce the size of the required maneuver. The initial conditions at the Titan flyby are parameterized as,

v_∞, α, β	Right ascension and declination of the outgoing V_∞ vector (bounded values).
$\phi = 0$	True anomaly (fixed value).
$r_{pmin} = 3,875$ km	Minimum flyby radius (minimum flyby altitude of 1,300 km, fixed value).
$\theta \in [0, 2\pi]$	Signed angle between the B-Plane coordinates T and B (bounded values).

Then, the appropriate set of initial conditions is generated by uniformly sampling the ranges of the free flyby parameters, that is, magnitude, right ascension and declination of the outgoing V_∞ vector, and θ. Additionally, the resulting trajectories are filtered based on additional constraints:

- The radius of periapsis after the flyby (r_p^+) in Saturn-centered coordinates must be less than the minimum impact radius.
- The orbital inclination after the flyby (i^+) must be limited such that the incoming trajectory does not intersect the rings or impact any icy moons.
- The orbital inclination before the flyby (i^-) must be limited to remain in a plane close to that of the spacecraft's reference trajectory orbital plane.

The constrained parameters i^+, r_p^+ and i^- can be estimated using the flyby state propagated in a two-body model at the sphere of influence of Titan. However, third body effects are not considered in this conic propagation and the resulting states are no longer accurate when propagated in a three-body model including Titan's gravitational effect. That is, a two-body flyby state that ends on Saturn impact may no longer impact the planet when propagated in the Saturn-Titan CR3B model. This effect is illustrated in Figure 5, where the trajectories in red and black represent the conic and three-body paths, respectively. The key in this process is to quickly generate a suitable set of initial conditions without relaying on any numerical integration for the map generation. To be able to exploit conic approximations without the loss of fidelity when transitioning from one model to the other, pseudo-state theory [14] is applied to the computation of a conic path that approximates a three-body trajectory at the pseudo-sphere of influence (blue trajectory in Figure 5). Based on

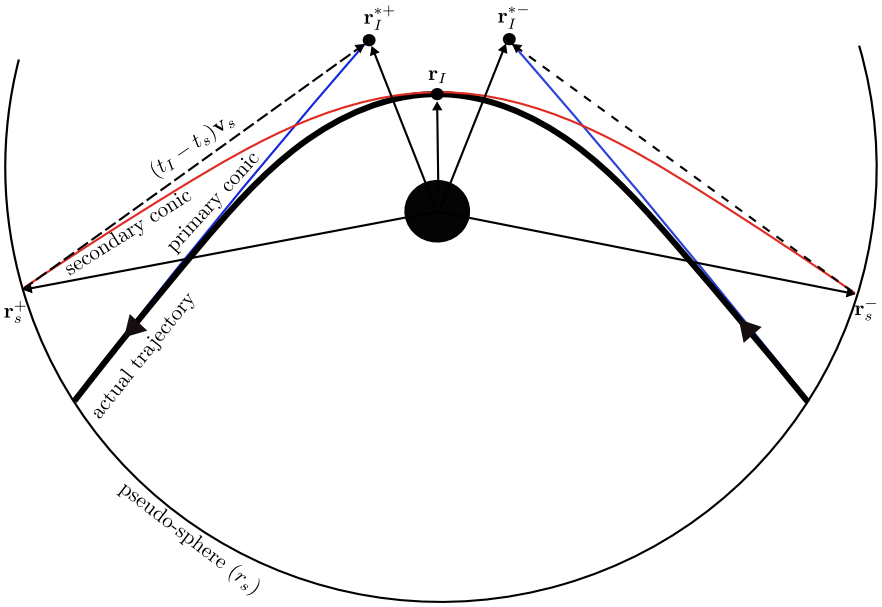

Figure 5. General representation of the pseudo-state mapping conics: the Saturn-centered primary conic is represented in blue, the Titan-centered secondary conic appears in red, and the actual trajectory propagated in a higher-fidelity model is shown in black.

pseudo-state theory mapping principles, for a given Titan-centered flyby state defined by $[t_I, \mathbf{r}_I, \mathbf{v}_I]$, there are two associated pseudo-states, before and after the flyby: $\mathbf{r}_I^{*+}$, $\mathbf{v}_I^{*+}$ and $\mathbf{r}_I^{*-}$, $\mathbf{v}_I^{*-}$, where the negative and positive upper scripts represent states before and after the flyby, respectively. These states can be computed using the pseudo-state mapping as follows[1],

Secondary conic pseudo-state	Primary conic pseudo-state
$\mathbf{r}_I^{*+} = \mathbf{r}_s^+ + (t_I - t_s^+)\,\mathbf{v}_s^+$	$\mathbf{R}_I^{*+} = R_{Titan} + \mathbf{r}_I^{*+}$
$\mathbf{v}_I^{*+} = \mathbf{v}_s^+$	$\mathbf{V}_I^{*+} = V_{Titan} + \mathbf{v}_I^{*+}$

where,

t_s^{+-}, $\mathbf{r}_s^{+-}$, $\mathbf{v}_s^{+-}$	Titan-centered state at the pseudo-sphere of influence pre(-)/post(+) flyby
t_I, $\mathbf{r}_I$, $\mathbf{v}_I$	Saturn-centered flyby state
t_I, $\mathbf{r}_I^{*+-}$, $\mathbf{v}_I^{*+-}$	Titan-centered pseudo-state after (+) or before (-) the flyby
t_I, $\mathbf{R}_I^{*+-}$, $\mathbf{V}_I^{*+-}$	Saturn-centered pseudo-state after (+) or before (-) the flyby
R_{Titan}, V_{Titan}	Saturn-centered Titan's state at the flyby time

allowing for the straightforward computation of i^+ and r_p^+ from t_I, $\mathbf{R}_I^{*+}$, $\mathbf{V}_I^{*+}$ and i^- from t_I, $\mathbf{R}_I^{*-}$, $\mathbf{V}_I^{*-}$. Once the set of initial conditions is selected, the next step in the process is the construction of the hyperplane Σ that defines the map. In this study, Σ is located such that $y = 0$, which is a common and widely used definition. Once the surface of section is defined and the set of appropriate initial

[1]The same expressions can be used to calculate the pseudo-states before the flyby.

states constructed, then states are integrated backward in time and the returns to the map of each trajectory are recorded and plotted using a combination of position and velocity states, i.e., $x - \dot{x}$. The resulting one-sided maps appear in Figure 6: Figure 6(a) represents the 'positive' map ($\dot{y} > 0$) and Figure 6(b) corresponds to trajectory crossings with $\dot{y} < 0$ ('negative' map). Every colored dot on the map, except for the gray-dots, represents a return of an impact trajectory to the map, that is, the six-dimensional state associated with each one of these dots, when propagated forward in time, results in an impact trajectory with Saturn and contains at the very least one controlled, or targeted, Titan flyby. Any other Titan flyby can certainly occur along the impact trajectory but is not controlled by the selection of the initial conditions. Further insight into the solution space can be gained by coloring the returns to the map based on the number of flybys associated with each individual impact trajectory. That is, the blue dots correspond to impact trajectories with at least one flyby, the magenta dots represent trajectories that impact Saturn after at least two Titan flybys, and the green dots, which are very few, hard to spot, and only appear in Figure 6(a), are associated with impact trajectories with three Titan flybys. Since the end goal is to connect one of these trajectories to the reference trajectory via an impulsive maneuver, of interest are returns to the map in the vicinity of the nominal reference trajectory crossings (to reduce the size of the required ΔV). For reference, the returns to the map of the reference trajectory appear as larger cyan dots.

It is also insightful to illustrate other dynamical structures at the energy level of the reference trajectory in the Saturn-Titan system; the returns of the impact trajectories to the map are plotted against a background Poincaré map (gray) that includes some of these structures. The non-dimensional initial conditions used to generate the background surface of section are selected to result in general dynamical structures for illustration purposes only, i.e., $x_0 = [-1.5 : 0.05 : -0.1]$, $\dot{x}_0 = [-0.5 : 0.01 : 0.5]$, $y_0 = z_0 = \dot{z}_0 = 0$. The corresponding value of $\pm\dot{y}_0$ is calculated directly from the expression for Jacobi constant associated with the reference path in this dynamical model ($C = 2.09$). Note that all of the returns to the map plotted in gray correspond to trajectories at the same energy level, i.e., the associated value of the Jacobi constant is the same. The Poincaré map is shown on the background of the impact map (blue, green, cyan, and magenta map) to provide context, but it is important to note that the associated trajectories are not at the same energy level, meaning that an intersection on the map is not necessarily an intersection in phase space and, thus, a maneuver is likely needed to connect two nearby trajectories. When propagating the initial conditions, longer integration times are necessary to produce sufficient crossings to yield a dense and well-defined map. In this particular case, an integration time of approximately one year is employed to generate the background map plotted in gray in Figure 6. Note that the initial conditions for the impact map are numerically integrated for approximately four months. The structures in Figure 6 display areas of periodic, quasi-periodic, and chaotic motion, bounding the motion in certain regions and highlighting areas of instability. The insight into the general design space is gained at this point in the process, allowing the designer to quickly evaluate different impact trajectories by exploring various regions on the maps. Once a suitable impact trajectory is identified, a differential corrector is employed to produce a trajectory that is continuous in position and velocity except at a connecting patch point between the reference path and the impact trajectory, where a ΔV is applied to join the two arcs. Although these maps offer a wide variety of impact trajectories ranging in time-of-flight and ΔV, only a small – but representative – subset is presented in Figure 7.

The time-of-flights associated with these sample impact trajectories are relatively short and well

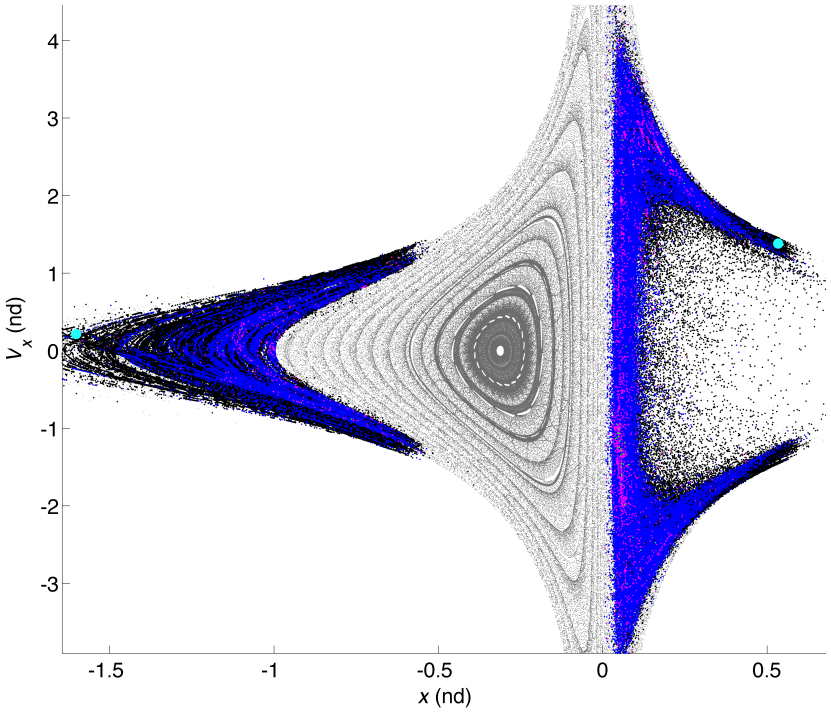

(a) Positive One-Sided Map ($\dot{y} > 0$)

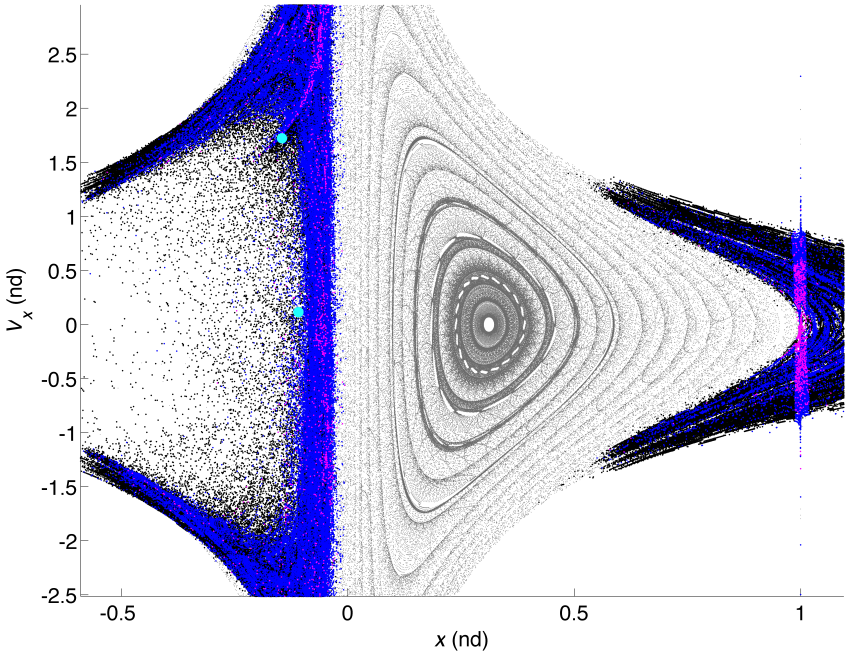

(b) Negative One-Sided Map ($\dot{y} < 0$)

Figure 6. Impact Maps with Saturn located at $(-\mu, 0)$ and Titan at $(1-\mu, 0)$: the cyan dots represent the returns of the nominal reference trajectory to the map, the gray dots display general periodic and quasi-periodic bounded behavior at this particular energy level, and the colored dots represent impact trajectory with one, two, and three Titan flybys.

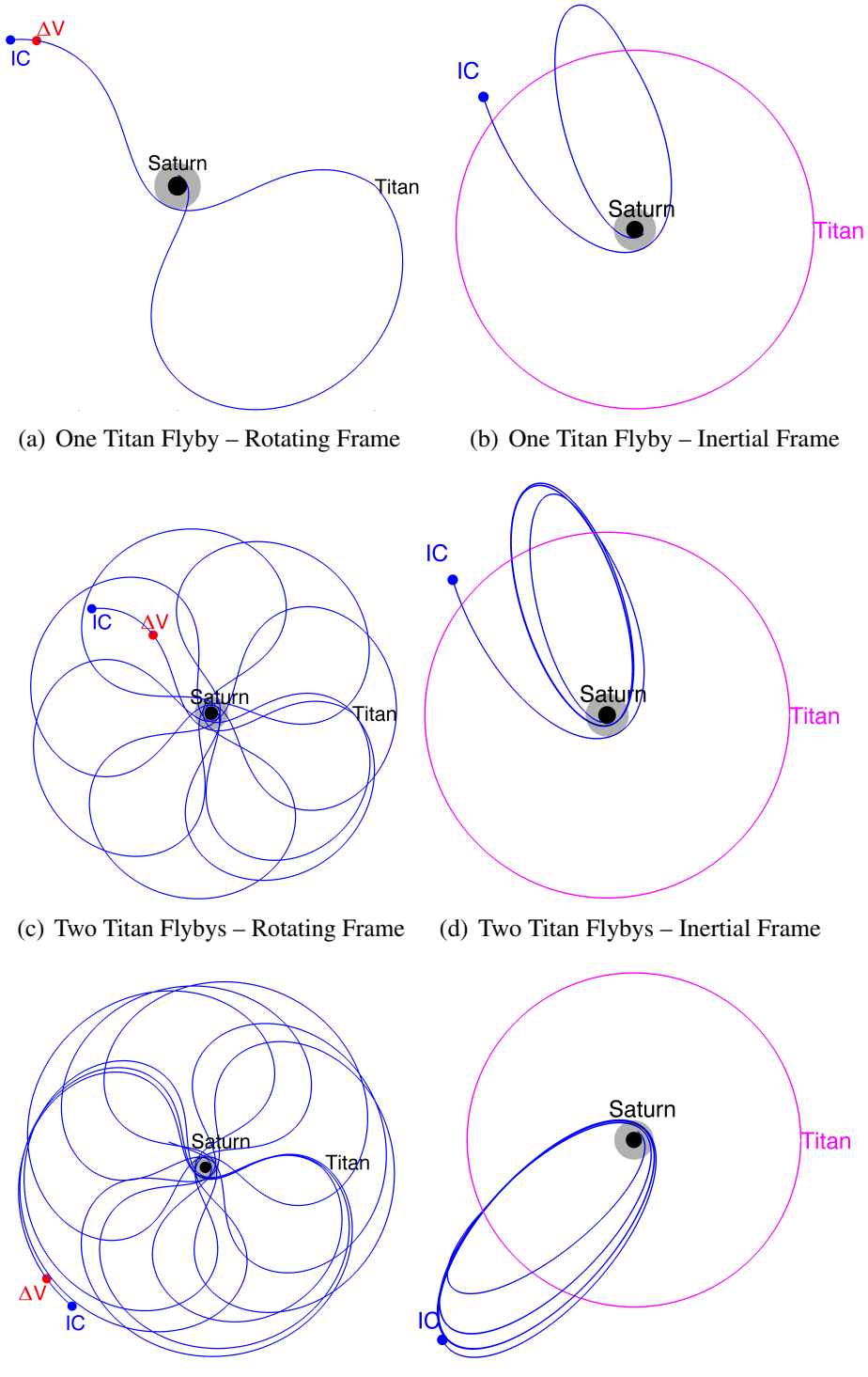

(a) One Titan Flyby – Rotating Frame (b) One Titan Flyby – Inertial Frame

(c) Two Titan Flybys – Rotating Frame (d) Two Titan Flybys – Inertial Frame

(e) Three Titan Flybys – Rotating Frame (f) Three Titan Flybys – Inertial Frame

Figure 7. Sample impact trajectories with one, two, and three Titan flybys plotted in the rotating and inertial frames. The red dot indicates the maneuver location and the blue dot represents the initial state on the reference trajectory. Titan's orbit is plotted in magenta and Saturn's rings in gray.

below the six month time-of-flight constraint: 10.9 days, 71.8 days, and 125.1 days for the impact trajectories with one, two, and three Titan flybys, respectively. Recall that the objective of this part of the analysis is not to produce ΔV-optimal nor flyable trajectories, but rather to quickly gain insight into the design space and the availability of possible solutions. Nevertheless, it is worth noting that the ΔV magnitude associated with all three trajectories is below 75 m/s. The one and two Titan flyby solutions illustrated in Figures 7(a)-7(b) and Figures 7(c)-7(d) are obtained from the map in Figure 6(b), whereas the three Titan flyby solution in Figures 7(e)-7(f) is computed from the map in Figure 6(a). Note that other solutions with different resonant and non-resonant arcs are available from the map but these three impact trajectories serve as illustrating examples; however, no solutions with more than three Titan flybys are identified due to imposed TOF and flyby altitude control restrictions.

Of course, there are limitations to the use of these maps. The biggest drawback is the lack of control over the second and third Titan flybys, which limits the leverage on the reduction of the ΔV. As expected, any single flyby trajectory, such as the one illustrated in Figures 7(a)-7(b), will meet the full set of constraints, but the associated propellant cost exceeds the limit. It is clear that more than one Titan flyby is needed to reduce the ΔV, but since there is no control over any subsequent flyby, many of the resulting multi-flyby trajectories violate the ring crossing constraint. Selecting initial conditions that yield multiple targeted flyby trajectories is a topic for future investigation. Yet, the maps, as constructed in this study, are useful and insightful, allowing the designer to quickly assess the solution space from a qualitatively perspective. Inevitably, a refined search is needed to fine-tune these impact trajectories.

3.2. Refined Search: Feasible, Optimal, Multi-Flyby Impact Trajectories

The next step in the design process consists of 1) approximating a multi-flyby solution by a series of patched-conic flybys and 2) using this solution as an initial guess to the multiple-shooting optimization problem. While the generation of patched-conic solutions is computationally cheap, the use of high-fidelity gravity models and the application of the full set of constraints make the second step in the refined search process computationally expensive.

3.2.1. Generation of Patched-Conic Solutions

A directed graph (a set of nodes connected by edges with a specific direction) serves as a method to represent patched-conic solutions: each node on the graph contains the incoming V_∞ vector and the epoch of closest approach of the flyby and each edge contains the outgoing V_∞ vectors connecting two nodes. The first node (root) in the graph consists of a set of initial conditions: incoming V_∞ vector, $\mathbf{v}_\infty^-$, and flyby epoch, t_{fb}. The initial conditions are obtained from the spacecraft reference trajectory at a particular flyby. Then, from the initial conditions, new nodes are generated by using three basic, well-known, numerically stable algorithms that produce non resonant, resonant, and π-transfer arcs [15]. New nodes are further expanded using the same algorithms and a sequence is obtained by traversing the graph until a controlled impact is achieved with Saturn or one of the selected Saturn's non-icy moons . Without any additional constraints, the directed graph grows exponentially and traversing all the possible solutions becomes an almost impossible task. Consequently, it is important to impose constraints when generating the graph. For instance, the

Table 1. Multiple-shooting optimization problem variables

Initial leg	guess	variable	bounds
Initial epoch	t_0	fixed	
Coast time	0	free	$0 \leq \Delta t < t_{fb1} - t_0$
Correction maneuver	$\Delta \mathbf{v}$	free	
Flyby legs			
Flyby epoch	t_{fbi}	free	
Outgoing V_∞ vector	$\mathbf{v}_{\infty i}^{+}$	free	
Flyby altitude	h_i	free	$h_{min} \leq h_i$
Signed angle between B-Plane coordinates, T and B	θ_i	free	$\theta \in [0, 2\pi]$
True anomaly	0	fixed	
Impact leg			
Coast to impact	$\Delta t_{impact} = 1$ day	free	$\Delta t_{min} \leq \Delta t_{impact} \leq \Delta t_{max}$

number of maximum flybys in the sequence, the maximum time-of-flight or the minimum flyby altitude are parameters to be limited. The number of new nodes generated by each algorithm must also be constrained. While the non-resonant and π-transfer algorithms produce a finite number of nodes (solutions), the resonant transfer algorithm generates a bounded set of infinite solutions. These solutions can be parameterized by a single variable: the delta-crank angle ($-\Delta k_{max} \leq \Delta k \leq \Delta k_{max}$) or flyby altitude ($h_{min} \leq h \leq h_{max}$). These parameters are then used to search for solutions that minimize the radius of periapsis of the trajectory after a flyby while avoiding any ring crossing, reducing the number of solutions generated by the resonant strategy and, hence, reducing the size of the solution graph.

3.2.2. Solving the Multiple-Shooting Optimization Problem

A candidate solution sequence, found by traversing the graph generated in the previous step, is composed of an ordered list of flyby epochs and incoming and outgoing V_∞ vectors. Each element of the list is employed to create a control point in the multiple-shooting optimization problem defined in Section 2.2.1. Additionally, it is necessary to define an arc that connects the reference trajectory to the candidate solution. To do so, the spacecraft reference trajectory is propagated to a given future epoch – prior to the nominal flyby epoch – where a correction maneuver is applied. At this state, the spacecraft trajectory transitions from the reference to the new impact trajectory. For reference, the variables associated with the initial leg (up to the point where the correction maneuver is applied) and the variables associated with each subsequent flyby are displayed in Table 1. Once an initial guess is constructed, continuity in time, position, and velocity are enforced between control points. Additional constraints are applied to ensure that the trajectory ends on Saturn (or a selected moon) impact.

The simulation environment in which the problem is solved needs to be accurately defined. In this study, the gravity field is composed of the Sun, Saturn (including J2 and J4 terms), Mimas, Rhea, and Titan, and the Copernicus software tool [16] with the SnOpt optimizer [17] serves as the platform for the problem formulation. Due to the simplified gravity model used in the patched-conic

approximation, not all the candidate sequences generated in step 1 can be converged in the high-fidelity environment. As expected, when the trajectory approaches Saturn, the J2 and J4 coefficients in Saturn's gravity model make the flyby epochs predicted by the patched-conic solution off by several hours. This difference results in either a large correction maneuver or non-convergence by the optimizer.

Sample Saturn Impact Trajectory A representative feasible solution for a Saturn impact trajectory appears in Figure 8 plotted in a Saturn-centered inertial frame. This particular solution consists of four Titan flybys – three resonant and one non-resonant flyby transfers – culminating in Saturn impact. By definition, in a Titan-to-Titan n:m resonant transfer, the time-of-flight is an integer multiple of Titan's period, where m represents the number of spacecraft orbits around Saturn and n is the number of Titan revolutions [18]. Consequently, the flybys at the beginning and end of a resonant transfer occur at approximately the same place in Titan's orbit. The longitude of the encounters occurs on a fixed line passing from Saturn to Titan and the resonant transfer may be inclined. In a non-resonant transfer, the time-of-flight is not an integer multiple of the gravity-assist body's orbit. Non-resonant flybys, therefore, occur at different longitudes in Titan's orbit. Because the flybys of a non-resonant transfer do not occur at the same longitude, the spacecraft's orbit plane is constrained to be the same as the gravity-assist body's orbit plane. The change in orbital period along the impact trajectory in Figure 8 is illustrated in Figure 9(b). After the first Titan flyby, T-1, the spacecraft's trajectory is in a 1:1 resonance with Titan; the second flyby, T-2, changes the orbital period to a 4:3 resonance, and the third flyby, T-3, transitions it to a 3:2 resonance. After the fourth flyby, T-4, the spacecraft is in a non-resonant path to Saturn impact. Note that the orbital elements before the time of the ΔV correspond to that of Cassini's reference trajectory.

The selected Saturn impact trajectory meets the full set of requirements: 1) it does not intersect the rings, i.e., the inclination of the final leg (impact arc after the last targeted Titan flyby) at the time of impact, with respect to the ring-plane inclination, is 6.48^o)[2], as illustrated in Figure 9(a), 2) it does not intersect the the path of any of the considered moons (those included in the gravity field, i.e., Rhea, Mimas, and Titan), and 3) it is ΔV-optimal. The change in radius of periapsis is shown in Figure 9(c). For reference, the dotted blue line highlights the impact radius considered in this study. The first flyby raises the radius of periapsis to avoid undesired ring-plane crossings, but subsequent flybys are exploited to reduce the impact trajectory's r_p down to the desired radius. For completeness, the table provided in Figure 8 lists the radius and epoch associated with ascending and descending ring-plane crossings of the impact trajectory (with radius less than 500,000 km), and it is apparent that none of them are close to the F-ring radius of 140,000 km. The size of the correction maneuver is 3.998 m/s and the total time-of-flight is 88.66 days.

Sample Moon Impact Trajectory A representative feasible solution for a Mimas impact trajectory appears in Figure 10. This particular trajectory consists of only one non-resonant Titan flyby at an altitude of 2,206 km, as shown in Figure 11(b). The size of the required correction maneuver is 11.763 m/s and the total time-of-flight to impact is 18.32 days. Figure 11(a) shows the change in

[2]The distance to the F-ring – 140,000 km – drives the ring-plane crossing constraint.

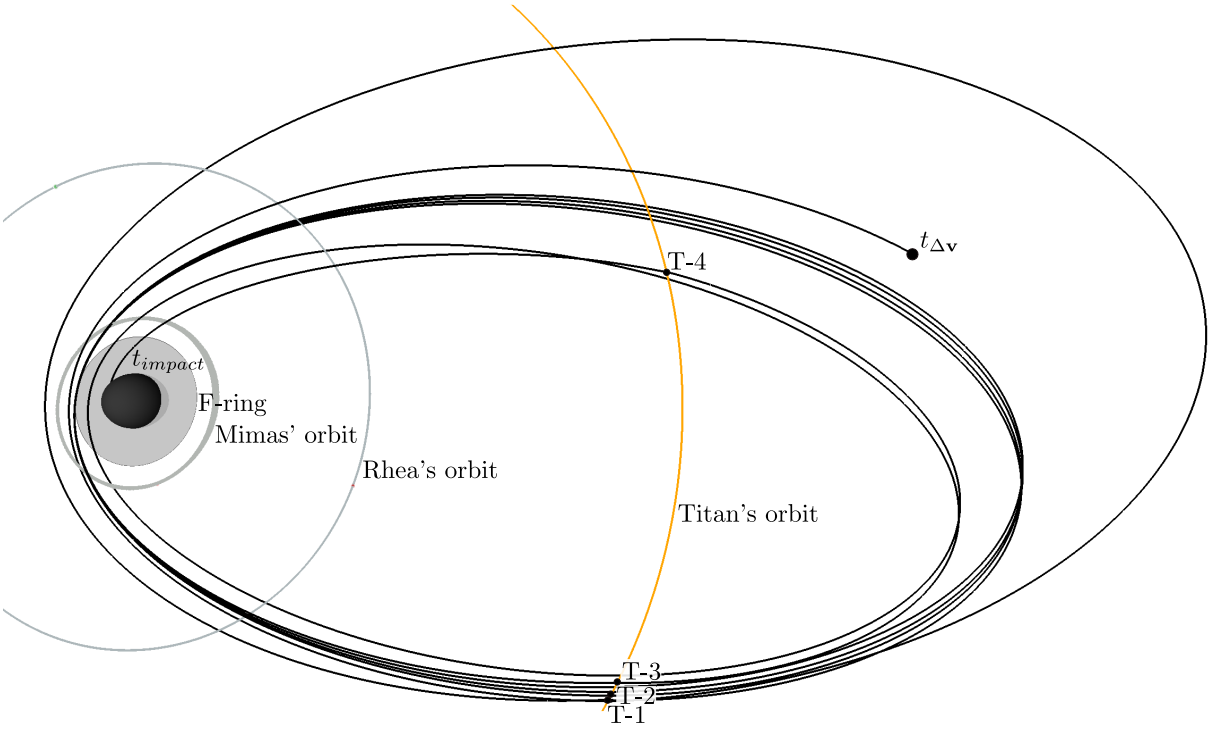

(a) Top view

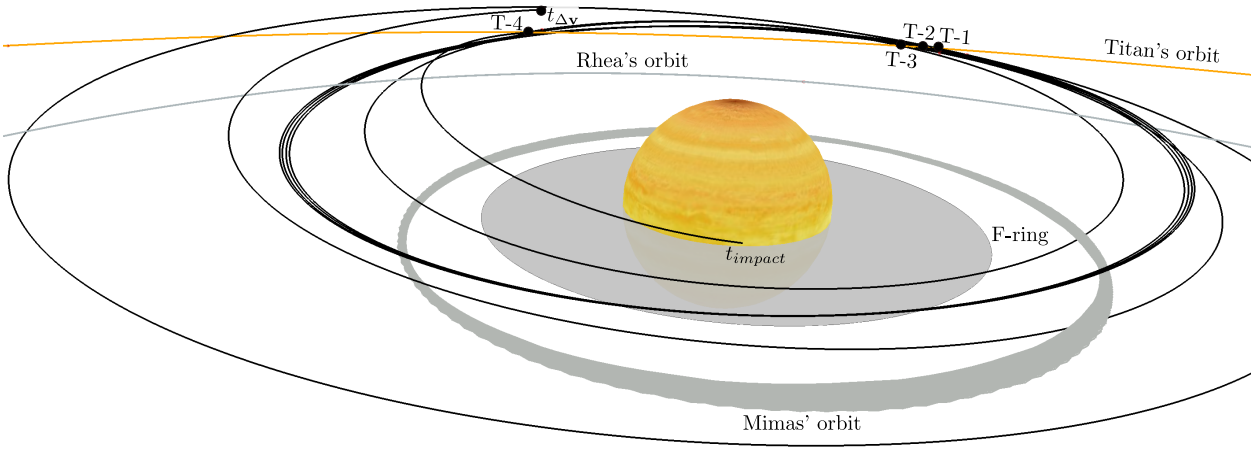

(b) Side view

Figure 8. Four Titan flyby impact trajectory with Saturn plotted in a Saturn-centered inertial frame.

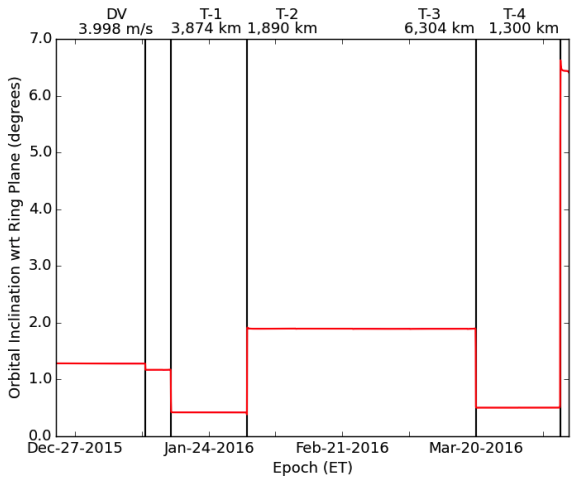

(a) Orbital Inclination vs. Time

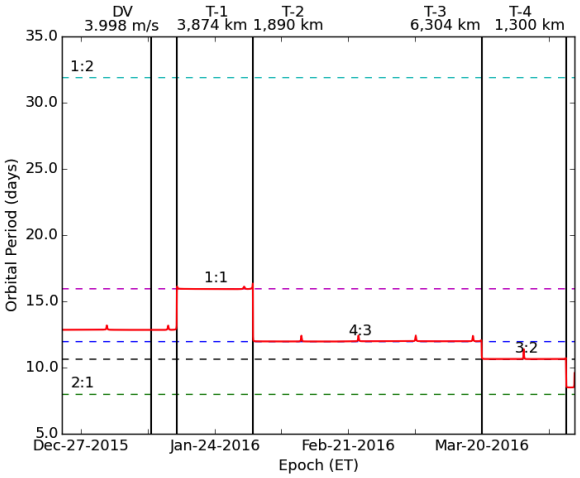

(b) Orbital Period vs. Time

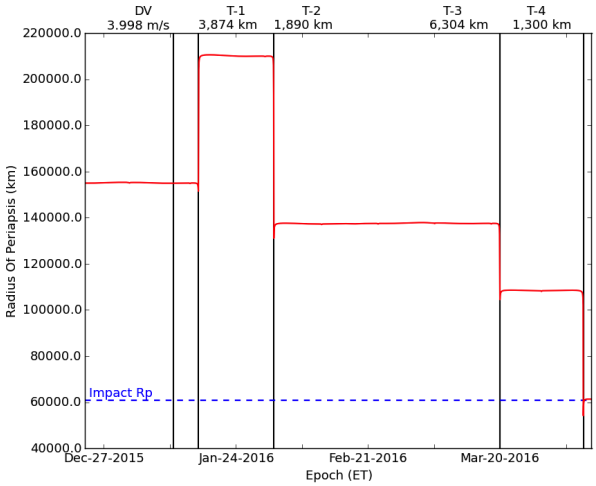

(c) Radius of Periapsis vs. Time

Ring Plane Crossing (RPC)	Radius (km)	Epoch (ET)	
Des. RPC – 1	221,188	30-JAN-2016	06:18
Asc. RPC – 2	150,249	11-FEB-2016	03:19
Asc. RPC – 3	151,318	23-FEB-2016	02:20
Asc. RPC – 4	152,390	06-MAR-2016	02:04
Des. RPC – 5	153,086	18-MAR-2016	01:44
Asc. RPC – 6	307,623	28-MAR-2016	12:55
Des. RPC – 7	150,278	28-MAR-2016	20:04

**RPC radius < 500,000 km

(d) Ring-Plane Crossings Radii and Epochs

Figure 9. Osculating orbital elements as a function of time associated with the Saturn impact trajectory illustrated in Figure 8. For reference, the epochs associated with the correction maneuver and each of the four Titan flybys are represented by vertical solid black lines.

orbital inclination with respect to the ring plane; at the time of impact, the inclination is 0.7^o. Other one-flyby solutions with the other moons are available but omitted for brevity.

4. Summary of Findings and Conclusions

The possibility of a premature end-of-mission is a common concern amongst mission designers, especially in mission scenarios involving pristine environments with strict planetary protection requirements. A robust and efficient design method to quickly produce viable terminating trajectories is presented in this paper. The proposed design process involves two separate, independent approaches: an initial assessment of the global solution space by exploiting mapping techniques combined with pseudo-state theory in the Saturn-Titan Circular Restricted Three-Body Problem

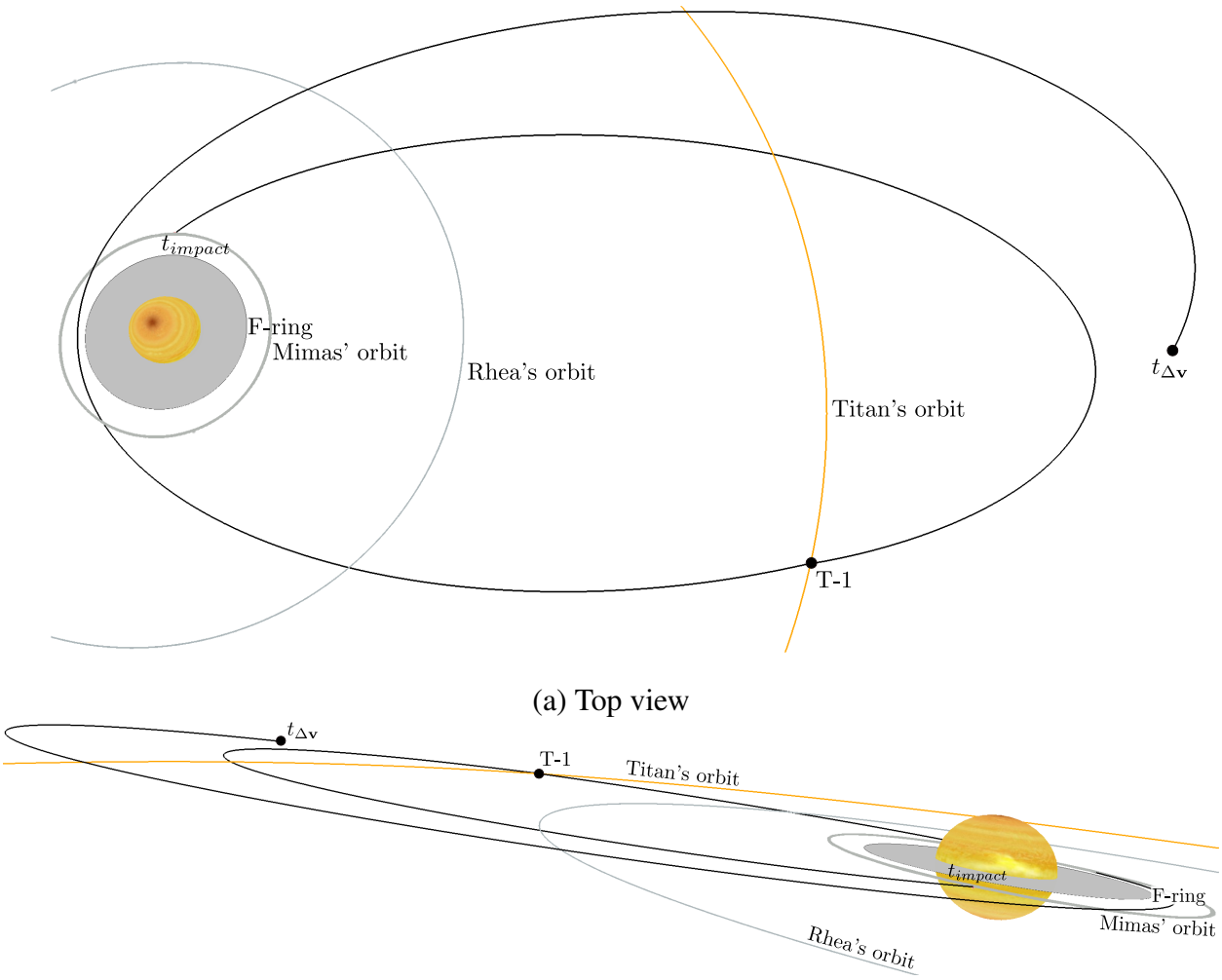

(a) Top view

(b) Side view

Figure 10. One Titan flyby impact trajectory with Mimas plotted in a Saturn-centered inertial frame.

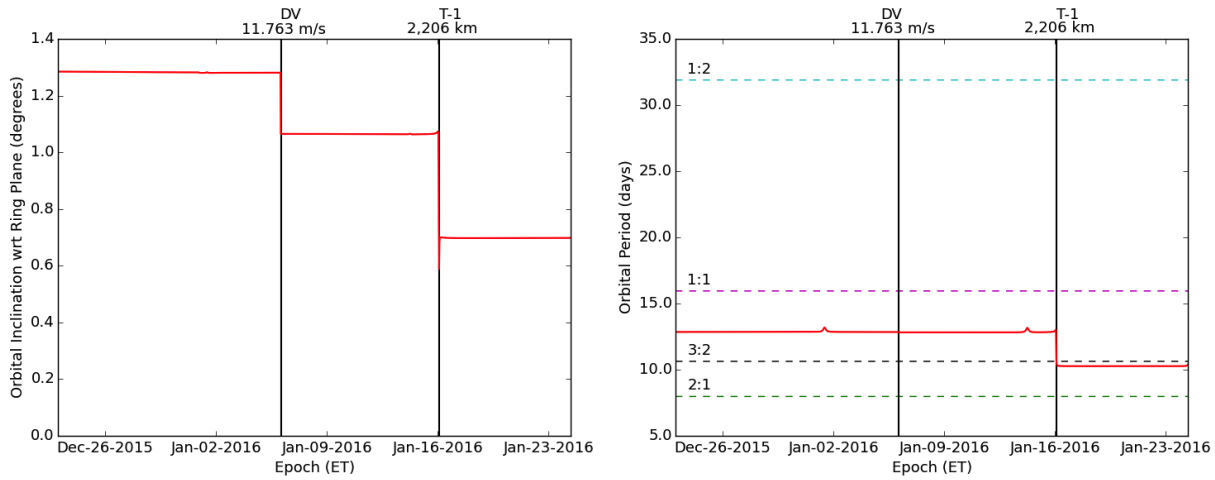

(a) Orbital Inclination vs. Time

(b) Orbital Period vs. Time

Figure 11. Osculating orbital elements as a function of time associated with the Mimas impact trajectory illustrated in Figure 10. For reference, the epochs associated with the correction maneuver and the Titan flyby are represented by vertical solid black lines.

and a highly refined search method to produce individual, feasible point solutions that meet the full set of requirements and constraints for each specific mission scenario. Although the global method, as currently developed, does not produce flyable impact trajectories, it certainly offers much more insight into the general type of available solutions and allows the designer to quickly make general observations about the trade space in terms of number of flybys, required ΔV, and estimated time-of-flight to impact. The application of various mapping techniques to this problem is also advantageous allowing the dimensionality of the problem to be reduced and thousands of potential impact trajectories to be visualized on a condensed 2D surface of section. The highly successful Cassini mission serves as a working platform to illustrate the design process, but the proposed techniques can be easily applied to other spacecraft missions.

5. Acknowledgments

This research was carried out at the Jet Propulsion Laboratory, California Institute of Technology, under a contract with the National Aeronautics and Space Administration. Reference to any specific commercial product, process, or service by trade name, trademark, manufacturer or otherwise, does not constitute or imply its endorsement by the United States Government or the Jet Propulsion Laboratory, California Institute of Technology. The authors thank Duane Roth, Earl Maize, Brent Buffington, and Yungsun Hahn for providing valuable insight into the problem and reviewing this work.

6. References

[1] Buffington B., Smith J., Petropoulos A., Pelletier F., and Jones J. “Proposed End-Of-Mission for the Cassini Spacecraft: Inner D Ring Ballistic Saturn Impact.” “61st International Astro-

nautical Congress," Prague, CZ, September 27 – October 1, 2010.

[2] C. H. Yam, D. C. Davis, J. M. Longuski, and K. C. Howell. "Saturn Impact Trajectories for Cassini End-of-Mission." Journal of Spacecraft and Rockets, DOI:10.2514/1.38760. 2008.

[3] C. Patterson, M. Kakoi, K. C. Howell, C. H. Yam, J. M. Longuski. "500-Year Eccentric Orbits for the Cassini Spacecraft within the Saturnian System." AAS/AIAA Astrodynamics Specialist Conference, AAS Paper 07-256. Mackinac Island, Michigan, August 19–23 2007.

[4] Smith, J. and Buffington, B. "Overview of the Cassini Solstice Mission Trajectory." "AAS/AIAA Astrodynamics Specialist Conference, AAS Paper 09-351," Pittsburg, PA, August 18–21, 2009.

[5] V. Szebehely. Theory of Orbits: The Restricted Problem of Three Bodies. Academic Press, Inc., New York, New York, 1967.

[6] T. A. Pavlak. "Mission Design Applications in the Earth-Moon System: Transfer Trajectories and Stationkeeping." M.S. Thesis, School of Aeronautics and Astronautics, Purdue University, West Lafayette, Indiana, 2010.

[7] D. J. Grebow. "Trajectory Design in the Earth-Moon System and Lunar South Pole Coverage." Ph.D. Dissertation, School of Aeronautics and Astronautics, Purdue University, West Lafayette, Indiana, 2010.

[8] M. Vaquero. "Spacecraft Transfer Trajectory Design Exploiting Resonant Orbits in Multi-Body Environments." Ph.D. Dissertation, School of Aeronautics and Astronautics, Purdue University, West Lafayette, Indiana, 2013.

[9] R. Battin. An Introduction to the Mathematics and Methods of Astrodynamics. American Institute of Aeronautics and Astronautics, 1987.

[10] M. Vaquero and K. C. Howell. "Transfer Design Exploiting Resonant Orbits and Manifolds in the Saturn-Titan System." Journal of Spacecraft and Rockets, February 2013. DOI: 10.2514/1.A32412.

[11] M. Vaquero and K. C. Howell. "Design of Transfer Trajectories Between Resonant Orbits in the Earth-Moon Restricted Problem." Acta Astronautica, May 2013. Available at: http://dx.doi.org/10.1016/j.actaastro.2013.05.006.

[12] D. C. Davis and K. C. Howell. "Trajectory Evolution in the Multi-Body Problem with Applications in the Saturnian System." Acta Astronautica, Vol. 69, pp. 1038–1049, 2011.

[13] A. F. Haapala and K. C. Howell. "Representations of Higher-Dimensional Poincaré Maps with Applications to Spacecraft Trajectory Design." "63rd International Astronautical Congress," Naples, Italy, October 1-5 2012. Paper IAC-12.C1.7.2.

[14] Wilson, S. "A Pseudostate Theory for the Approximation of Three-Body Trajectories." Tech. rep., MSC/TRW Task A-60.1, Mission Planning and Analysis Division NASA Manned Spacecraft Center, 1969.

[15] Strange, N., Russell, R., and Buffington, B. "Mapping the V-Infinity Vector." "Astrodynamics Specialist Conference. Mackinac Island, Michigan," August 19-23, 2007.

[16] Ocampo, C., Senent, J., and Williams, J. "Theoretical Foundation of Copernicus: A Unified System for Trajectory Design and Optimization." "4th International Conference on Astrodynamics Tools and Techniques. Madrid. Spain," 2010.

[17] Gill, P. E., Murray, W., and Saunders, M. A. "SNOPT: An SQP Algorithm for Large-Scale Constrained Optimization." SIAM Journal on Optimization, Vol. 12, p. 9791006, 2002.

[18] Murray, C. D. and Dermott, S. F. Solar System Dynamics. Cambridge University Press, Cambridge, Cambridge, United Kingdom, 1999.